



On the Viability of Magnetometer-Based Projectile Orientation Measurements

by Thomas E. Harkins

ARL-TR-4310

November 2007

NOTICES

Disclaimers

The findings in this report are not to be construed as an official Department of the Army position unless so designated by other authorized documents.

Citation of manufacturer's or trade names does not constitute an official endorsement or approval of the use thereof.

DESTRUCTION NOTICE—Destroy this report when it is no longer needed. Do not return it to the originator.

Army Research Laboratory

Aberdeen Proving Ground, MD 21005-5069

ARL-TR-4310

November 2007

On the Viability of Magnetometer-Based Projectile Orientation Measurements

Thomas E. Harkins

Weapons and Materials Research Directorate, ARL

Approved for public release; distribution is unlimited.

REPORT DOCUMENTATION PAGE

Form Approved
OMB No. 0704-0188

Public reporting burden for this collection of information is estimated to average 1 hour per response, including the time for reviewing instructions, searching existing data sources, gathering and maintaining the data needed, and completing and reviewing the collection information. Send comments regarding this burden estimate or any other aspect of this collection of information, including suggestions for reducing the burden, to Department of Defense, Washington Headquarters Services, Directorate for Information Operations and Reports (0704-0188), 1215 Jefferson Davis Highway, Suite 1204, Arlington, VA 22202-4302. Respondents should be aware that notwithstanding any other provision of law, no person shall be subject to any penalty for failing to comply with a collection of information if it does not display a currently valid OMB control number.

PLEASE DO NOT RETURN YOUR FORM TO THE ABOVE ADDRESS.

1. REPORT DATE (DD-MM-YYYY) November 2007		2. REPORT TYPE Final		3. DATES COVERED (From - To) 2001-2007	
4. TITLE AND SUBTITLE On the Viability of Magnetometer-Based Projectile Orientation Measurements				5a. CONTRACT NUMBER	
				5b. GRANT NUMBER	
				5c. PROGRAM ELEMENT NUMBER	
6. AUTHOR(S) Thomas E. Harkins (ARL)				5d. PROJECT NUMBER 1L162618AH80	
				5e. TASK NUMBER	
				5f. WORK UNIT NUMBER	
7. PERFORMING ORGANIZATION NAME(S) AND ADDRESS(ES) U.S. Army Research Laboratory Weapons and Materials Research Directorate Aberdeen Proving Ground, MD 21005-5066				8. PERFORMING ORGANIZATION REPORT NUMBER ARL-TR-4310	
9. SPONSORING/MONITORING AGENCY NAME(S) AND ADDRESS(ES)				10. SPONSOR/MONITOR'S ACRONYM(S)	
				11. SPONSOR/MONITOR'S REPORT NUMBER(S)	
12. DISTRIBUTION/AVAILABILITY STATEMENT Approved for public release; distribution is unlimited.					
13. SUPPLEMENTARY NOTES					
14. ABSTRACT Vector magnetometers are being widely considered for roll orientation estimation in a number of guided projectile programs. The U.S. Army Research Laboratory (ARL) has included vector magnetometers in inertial sensor suites in several hundred projectile test and evaluation flight experiments since the mid 1990s. Based on analyses and experiences with these devices, circumstances affecting magnetometer-based measurements have been identified and investigated. Results of these analytic and experimental efforts will be presented to support the conclusion that vector magnetometers are viable roll orientation sensors when properly employed.					
15. SUBJECT TERMS guided projectiles; high g; magnetic sensor; magnetometers; projectile navigation					
16. SECURITY CLASSIFICATION OF:			17. LIMITATION OF ABSTRACT	18. NUMBER OF PAGES	19a. NAME OF RESPONSIBLE PERSON
a. REPORT Unclassified	b. ABSTRACT Unclassified	c. THIS PAGE Unclassified	SAR	35	Thomas E. Harkins
			19b. TELEPHONE NUMBER (Include area code) 410-306-0850		

Contents

List of Figures	iv
List of Tables	iv
1. Introduction	1
2. Deriving Projectile Angles With Magnetometers	2
3. Does the Geomagnetic Field Always Provide Roll Position?	5
3.1 Occasions When Radial Magnetometers Do Not Provide a Roll-Modulated Signal.....	6
3.2 Error Magnitudes In Roll Angle Computations	7
4. Sensor Survivability	11
5. Real-Time, On-Board Solution of the Roll Equations	12
5.1 Explicit Solution.....	12
5.2 Projectile-Dynamics-Dependent Methods	14
6. Non-Geomagnetic Field Sensor Stimuli	15
6.1 Projectile-Independent Magnetic Fields.....	15
6.2 Projectile-Related Magnetic Fields	17
7. Summary	24
8. References	25
Distribution List	26

List of Figures

Figure 1. Coordinate systems.....	2
Figure 2. Earth-fixed, navigation, and body-fixed systems and the Euler angle rotations.....	4
Figure 3. Geomagnetic field and Euler angles relating local field vector and radial magnetometer axis.....	5
Figure 4. Representative radial magnetometer output.....	6
Figure 5. $\partial\phi_M/\partial\theta$ at APG.....	8
Figure 6. $\partial\phi_M/\partial\psi_N$ at APG.....	9
Figure 7. RSS of $\partial\phi_M/\partial\theta$ and $\partial\phi_M/\partial\psi_N$	9
Figure 8. RSS in region of sensitivity.....	10
Figure 9. M831 with diagnostic fuze after 49-Kg launch and magnetometer-derived roll rate. .	12
Figure 10. Mag_J output inside range.....	17
Figure 11. Mag_J output outdoors.....	16
Figure 12. Diagnostic fuze.....	17
Figure 13. Magnetometer data taken with spin motor.....	17
Figure 14. Magnetometer saturation attributable to projectile permanent magnetism.....	17
Figure 15. Two magnetometers in a rotating field.....	18
Figure 16. Canard control motor.....	19
Figure 17. Depth of penetration as a function of frequency.....	19
Figure 18. Flux in and around a solid cylinder rotating in a stationary magnetic field.....	20
Figure 19. DFuze with two magnetometers.....	20
Figure 20. Cylindrical test fixture specifications.....	21
Figure 21. Effect of spin rate on magnetometer output amplitude.....	21
Figure 22. Representative magnetic and solar sensor data from spin effects tests.....	23
Figure 23. Magnetometer output lag versus spin rate for various materials.....	23
Figure 24. Embedded magnetometer lags for two stainless steel cylinders.....	24

List of Tables

Table 1. Error sensitivity of roll angle computations.....	10
Table 2. Error sensitivity of roll angle computations for artillery and tanks at APG.....	11

1. Introduction

Accurate position and heading information are required for successful navigation. In particular, when dealing with rolling projectiles, we must know the roll orientation in order to properly execute desired maneuvers. Requirements for on-board sensors imposed by military applications such as non-emitting sensors, high-g survivability, low cost, low power consumption, high spin rates, and small size exclude many traditional roll orientation measurement systems. Recent advances in magnetic sensor technologies have resulted in devices that operate effectively in the military ordnance environment and are capable of making high-speed, high-resolution measurements of sensor attitude relative to the earth's magnetic field when installed on freely flying bodies. The U.S. Army Research Laboratory (ARL) has included vector magnetometers in inertial sensor suites in several hundred projectile test and evaluation flight experiments since the mid 1990s. Projectile heading and roll orientation histories are derived with the use of these magnetometer data in post-flight processing (Harkins, 2003, 2004, 2007; Hepner & Harkins, 2001; Wilson, 2004, 2005). Additionally, magnetometers have been successfully used for on-board, real-time projectile roll orientation determination in flight experiments of several projectile maneuver systems during controlled conditions.

Although these successes are noteworthy achievements, several questions need to be addressed before we conclude that magnetometers are viable roll sensors for guided projectiles. Since the derivation of roll information from magnetometer measurements depends on the solution of equations relating sensor output and sensor orientation with respect to the earth's magnetic field, these questions fall under four general headings. First, are the equations that describe this relationship robust? Second, does the hardware operate reliably and effectively in the anticipated tactical environment? Third, is solution of the equations describing this relationship practicable for applications of interest? Fourth, are there things that affect the relationship between sensor output and sensor orientation with respect to the earth's field in projectile applications? If so, can these occurrences be detected and corrected/compensated?

Following a brief description of how roll information is derived from magnetometer measurements, each of these questions is addressed in turn. I argue that the answer in each instance is yes, except in very limited cases. Therefore, I conclude that vector magnetometers are viable roll orientation sensors when properly employed.

2. Deriving Projectile Angles With Magnetometers

The formulation of solutions for projectile roll orientation from magnetic sensor data follows from the algebra relating the definitions of a vector describing the earth's magnetic field in multiple coordinate systems.¹ Three coordinate systems are typically used when one is dealing with inertial navigation problems for gun- and tube-launched projectiles.

The first system is a right-handed Cartesian system (I, J, K) with its origin at the launch site, which is used to describe trajectory time histories. This will be referred to as the “earth-fixed” system and the axes are defined by

- The I and J axes, which define a plane tangential to the earth's surface at the origin.
- The K axis, which is perpendicular to the earth's surface with positive downward, i.e., in the direction of gravity.
- The I axis, which is chosen so that the centerline of the launcher is in the I - K plane.

Down-range travel is then measured along the I axis, deflection along the J axis (positive to the right when one is looking down range), and altitude along the K axis (positive downwards) (see figure 1).

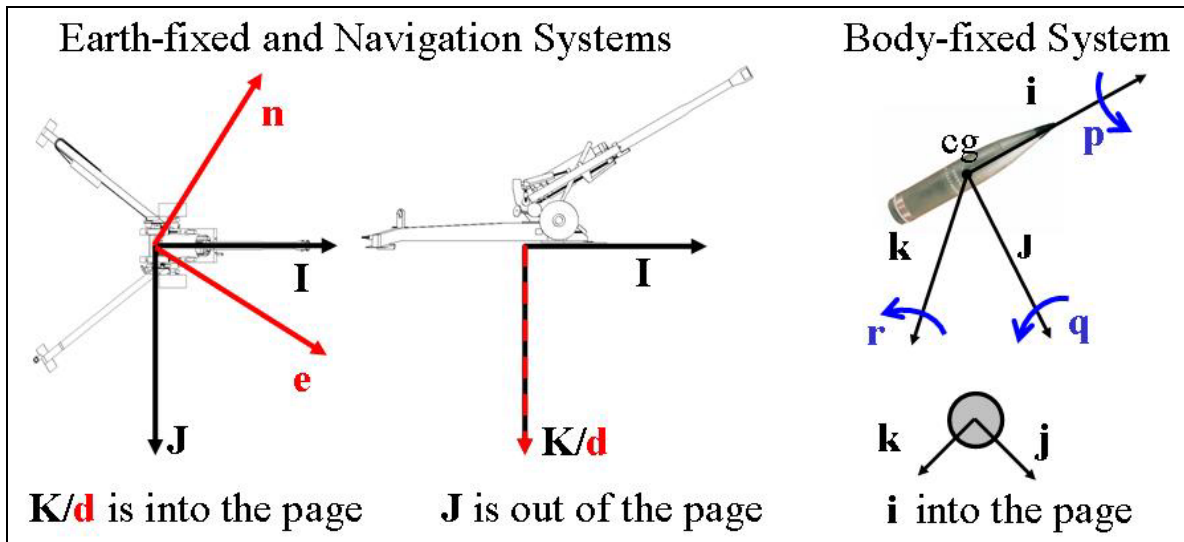


Figure 1. Coordinate systems.

¹Although the geomagnetic field varies over time and with location and altitude, it is essentially invariant over the durations and distances of most Army ordnance trajectories. For trajectories of sufficient duration and/or extent that the geomagnetic field differs during the trajectory, algorithms accounting for those changes can be devised, but that subject is beyond the scope of this report.

The second coordinate system (n, e, d) is commonly employed to specify locations on or near the earth's surface, i.e., north, east, and down. This will be referred to as the “navigation” system. The orientations of the navigation system and earth-fixed differ only by a single rotation about the vertical axis (see figure 1).

The third system is convenient for aeroballistic computations of rigid projectiles' flights and for describing the locations and orientations of such projectiles' components. This system is right-handed Cartesian (i, j, k) with its origin at the center of gravity (c.g.) of the flight body. For rotating flight bodies, the projectile-fixed coordinate system usually has its i axis along the projectile axis of symmetry, i.e., the spin axis (with positive in the direction of travel at launch). The j and k axes are then oriented so as to complete the right-handed orthogonal system (figure 1). Spin (p), pitch (q), and yaw (r) rates are measured about these axes. This will be referred to as the “body-fixed” system.

The earth-fixed and body-fixed coordinate systems are related through an Euler rotation sequence beginning with a rotation of the earth-fixed frame about the K axis through the yaw angle ψ . The system is then rotated about the new J axis through the pitch angle θ . Finally, the system is rotated about the i axis through the roll angle ϕ . The two systems are related by the direction cosine matrix (DCM), T_{Eb} , with the subscript denoting earth fixed to body fixed. This transformation matrix is

$$T_{Eb} = \begin{pmatrix} c_\psi c_\theta & s_\psi c_\theta & -s_\theta \\ c_\psi s_\theta s_\phi - s_\psi c_\phi & s_\psi s_\theta s_\phi + c_\psi c_\phi & c_\theta s_\phi \\ c_\psi s_\theta c_\phi + s_\psi s_\phi & s_\psi s_\theta c_\phi - c_\psi s_\phi & c_\theta c_\phi \end{pmatrix}, \quad (1)$$

where c_\bullet is $\cos(\bullet)$, and s_\bullet is $\sin(\bullet)$. Transformations between any two right-handed Cartesian systems can be similarly defined with appropriate values for the Euler angles. The DCM relating the navigation and body-fixed system, T_{Nb} , is given by equation 1 with the substitution of ψ_N for ψ . Figure 2 shows the three systems and the Euler angle relations between them.

When the navigation and body-fixed systems are identical (i.e., $\psi_N = 0$, $\theta = 0$, $\phi = 0$), the projectile i axis is pointed north, the j axis is pointed east, and the k axis is pointed down.

Among the many varieties of magnetic sensors, “vector” magnetometers are devices whose output is proportional to the magnetic field strength along the sensor's axis(es). When a tri-axial vector magnetometer is installed on board a projectile so that the sensor axes are parallel to the axes of the body-fixed system, the projections of the earth's magnetic field onto each of the sensor axes can be obtained with the T_{Nb} DCM.

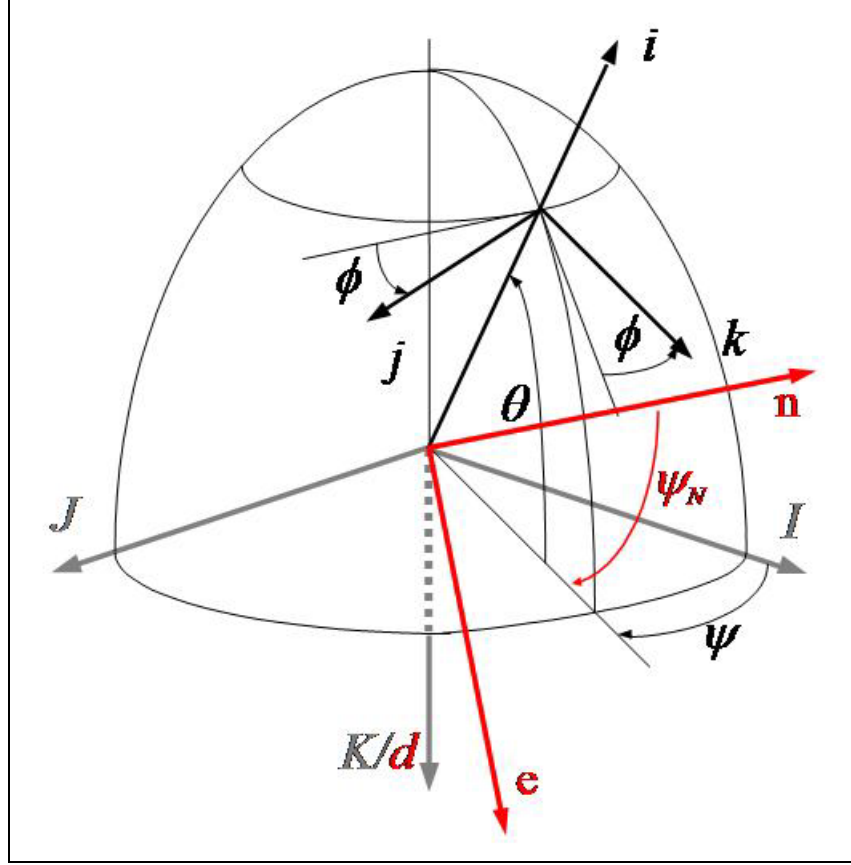


Figure 2. Earth-fixed, navigation, and body-fixed systems and the Euler angle rotations.

If $\vec{M}_N = (m_n, m_e, m_d)$ is the magnetic field vector in the navigation system, then the projections of the magnetic field vector along the sensor axes are given by

$$\vec{M}_b = T_{Nb} \vec{M}_N \quad (2)$$

with
$$m_i = \cos(\theta) \cos(\psi_N) m_n + \cos(\theta) \sin(\psi_N) m_e - \sin(\theta) m_d \quad (3)$$

$$m_j = [\sin(\theta) \sin(\phi) \cos(\psi_N) - \cos(\phi) \sin(\psi_N)] m_n + [\sin(\theta) \sin(\phi) \sin(\psi_N) + \cos(\phi) \cos(\psi_N)] m_e + \cos(\theta) \sin(\phi) m_d \quad (4)$$

$$m_k = [\sin(\theta) \cos(\phi) \cos(\psi_N) + \sin(\phi) \sin(\psi_N)] m_n + [\sin(\theta) \cos(\phi) \sin(\psi_N) - \sin(\phi) \cos(\psi_N)] m_e + \cos(\theta) \cos(\phi) m_d \quad (5)$$

Estimating projectile roll orientation with a radially oriented magnetometer fundamentally consists in solving equation 4 and/or equation 5 for ϕ . The particular means of achieving those solutions may vary from application to application, depending on anticipated projectile dynamics and the availability of data from other sensors. This is discussed further in section 5.

3. Does the Geomagnetic Field Always Provide Roll Position?

In any real magnetic sensor, determination of axes' orientations and calibration coefficients can be a complex process but for the present, I will assume an ideal tri-axial sensor whose output is given by equations 3, 4, and 5 in order to evaluate any inherent limitations in estimating roll with radial magnetometer data. Figure 3a illustrates the geomagnetic field which, on a large scale, is continuously changing in direction and amplitude but on the scale of travel of most Army projectiles, is invariant and can be described mathematically by a field of parallel vectors as illustrated in figure 3b.

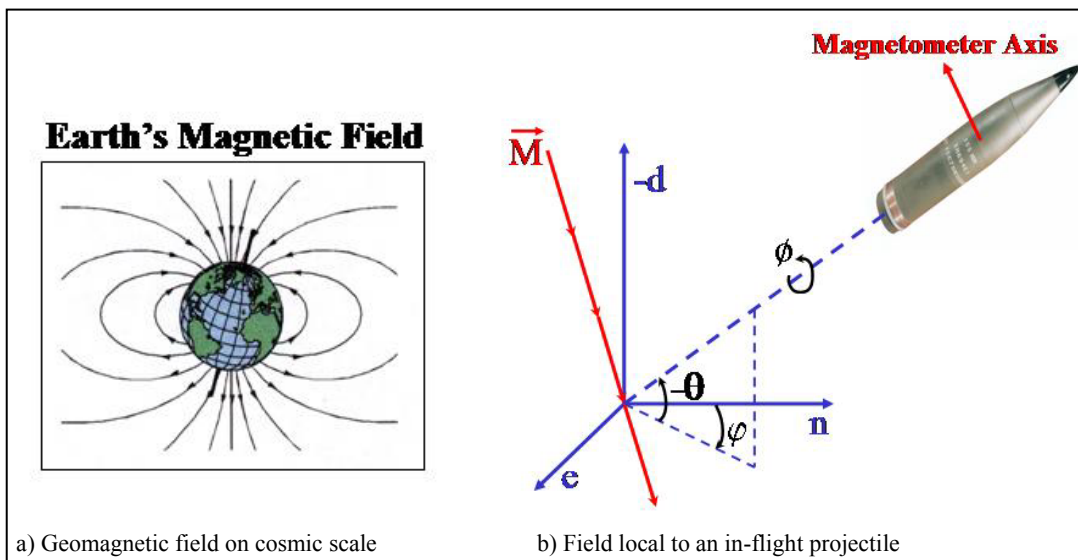


Figure 3. Geomagnetic field and Euler angles relating local field vector and radial magnetometer axis.

For a projectile whose spin rate is large with respect to the yawing rates, the time history of the projection of the local field vector onto a radially oriented magnetometer's axis would be a sinusoid whose amplitude varies directly with the magnetic aspect angle (σ_M), defined as the angle between the projectile spin axis and the local field vector. The frequency varies with the projectile spin rate. Figure 4 shows a representative portion of ideal output of the k axis-aligned sensor from a simulated trajectory. The signal from this sensor is referred to as Mag_K.

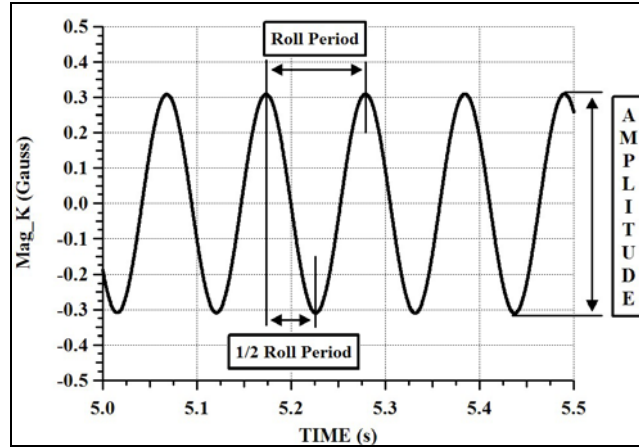


Figure 4. Representative radial magnetometer output.

3.1 Occasions When Radial Magnetometers Do Not Provide a Roll-Modulated Signal

With equation 5 giving the assumed perfect throughput of a k axis-aligned sensor, the theoretical limits on the accuracy of roll orientation estimates can be computed with the sensitivity and dynamic range specifications of a typical magnetic sensor. Logically, there are only three possible ways that a functioning, radially oriented, “vector” magnetometer on board a spinning body could fail to output a roll-modulated sinusoidal signal:

1. The spin axis is parallel to the local field.
2. The projectile is in lunar motion about the local field vector.
3. The field strength along the sensor axis is such that the sensor is either saturated or too small to register.

The first two possibilities describe geometries where the included angle between the sensor axis and the local field vector is constant. Although these are logical possibilities, they are not problems in any practical sense because both are statistical non-occurrences. Regarding the first case, every endo-atmospheric trajectory of any extent has curvature attributable to gravity-induced overturning and projectile drift. Thus, even if a projectile’s spin axis were at some time parallel to the magnetic field, this would be only a rapidly disappearing transient condition.

Regarding possibility 2, this is both a statistical non-occurrence for the reason just given and an aeroballistic non-occurrence for dynamically stable projectiles. Lunar motion requires the spin rate and coning rate to be equal. Rolling projectiles are specifically designed to avoid or minimize periods of such equality to prevent spin/yaw lock-in instabilities.

Regarding possibility 3, there are two related issues at play: sensitivity and/or quantization of the sensor and the dynamic range of the sensor. ARL has been successfully using Honeywell solid state vector magnetometers in flight instrumentation packages for more than 10 years. These devices have sensitivities on the order of 10 μ Gauss and a range of ± 6 Gauss. The earth’s field

varies between approximately 0.2 and 0.6 Gauss. When we do the math, unless the angle between the spin axis and the field vector is less than 0.0029 degree (i.e., $\sin^{-1} [.00001/.2]$), the sensor will have an analog response anywhere on earth to the geomagnetic field. ARL typically uses a 12-bit digital system with the sensor output scaled to a measurement range of ± 2 Gauss. In this setup, 1 bit = 4 Gauss/4096 = 0.00098 Gauss. When we do the math again, unless the angle between the spin axis and the field vector is less than 0.28 degree (i.e., $\sin^{-1} [.00098/.2]$), the sensor will have a digital response.

Recognizing the parallel spin axis case as a particular occurrence of the signal case being too small, we estimated the percentage of the sky where no digital response will occur in a 0.2-Gauss field from the ratio of the volumes of a unit height, 0.28-degree half-angle cone and a unit radius hemisphere. This ratio was computed to be 0.000019. Restated, the earth's field is observable in endo-atmospheric flight at least 99.99881% of the time with a radially oriented magnetometer such as those used at ARL.

The case of too great a signal (saturation) will occur only if there is an induced magnetic field approximately 10 times the earth's field. Of course, projectiles should not be made from materials that can be magnetized such as ferrous steel. Excluding that, can there be occasions when projectiles fly through external fields of sufficient magnitude to saturate a sensor? We have never seen this in a flight test but can one imagine such occurrences? Would saturation occur if a projectile were to fly along a power transmission line? I do not know but I suspect that even if the answer is yes, the occurrence rate is negligible. Besides, there are always other sensors with different ranges and sensitivities that might be employed in anticipated magnetic environments.

3.2 Error Magnitudes In Roll Angle Computations

Even though equations 4 and 5 have been shown to provide roll information at all times, the question remains, how good is that information in a realizable implementation? These equations may be algebraically solvable in the abstract to yield exact expressions for the roll angle (ϕ), but quantization errors in digital computations, estimation errors of the independent variables in these expressions, and inaccuracies in the knowledge of the local magnetic field are all unavoidable and contribute to errors in estimates of ϕ . To examine this error sensitivity, we will look at the computation of the roll position of the projectile when the k -axis aligned sensor (Mag_K) crosses the geomagnetic field.

With knowledge of the magnetic field, and knowledge of projectile elevation (θ) and azimuth (ψ_N), we can readily obtain the roll angle(s) at which Mag_K crosses the field (ϕ_M) by differentiating equation 5 and solving for the extrema of m_k . Alternatively, when we realize that when m_k is at a maximum or minimum, m_j is zero, the roll angles when Mag_K crosses the local field are given by solving equation 4 for ϕ with $m_j = 0$. Therefore,

$$\phi_M = \tan^{-1} \left(\frac{\sin(\psi_N) m_n - \cos(\psi_N) m_e}{\sin(\theta) \cos(\psi_N) m_n + \sin(\theta) \sin(\psi_N) m_e + \cos(\theta) m_d} \right) \quad (6)$$

Evaluating equation 5 at the principal value solution for ϕ_M will show whether Mag_K is at a maximum or minimum at that roll angle. This equation gives an exact analytical solution for ϕ_M , but the exact values of the independent variables θ, ψ_N, m_n, m_e , and m_d will seldom if ever be known. In order to examine sensitivity to these errors, a computer simulation was written wherein a magnetic field vector was defined and then the partial derivatives of equation 6 with respect to θ , i.e., $\partial\phi_M/\partial\theta$, and ψ_N , i.e., $\partial\phi_M/\partial\psi_N$, were evaluated at every potential projectile heading. Contour plots and tabular statistics were generated to describe the results.

For example, the geomagnetic field at Aberdeen Proving Ground (APG) is inclined approximately 67 degrees down from horizontal and declined 11 degrees west of north. When $\partial\phi_M/\partial\theta$ and $\partial\phi_M/\partial\psi_N$ are computed at 1-degree increments in azimuth ($0 \leq \psi_N \leq 360$) and elevation ($-90 \leq \theta \leq 90$), the contour plots shown in figures 5 and 6 result. The partial derivatives show that as the spin axis of a projectile approaches being parallel to the local field vector, the roll orientation solution equations become increasingly sensitive to errors in the independent variables. Figure 7 shows the root sum of squares (RSS) of $\partial\phi_M/\partial\theta$ and $\partial\phi_M/\partial\psi_N$. Figure 8 focuses on that portion of figure 7 where a projectile would be ascending and its spin axis is nearly parallel to the magnetic field. The contour lines are in increments of 1 degree of error in the roll angle computation per degree of error in the appropriate independent variable.

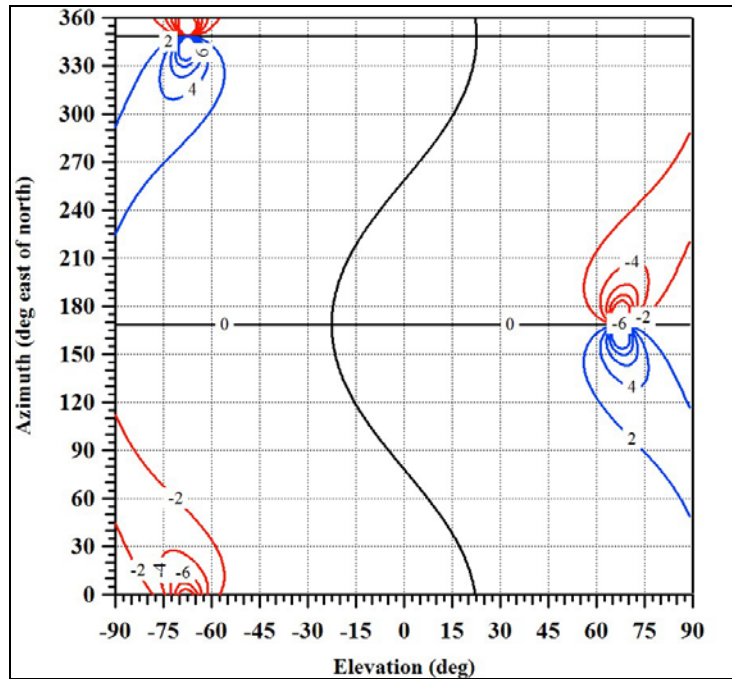


Figure 5. $\partial\phi_M/\partial\theta$ at APG.

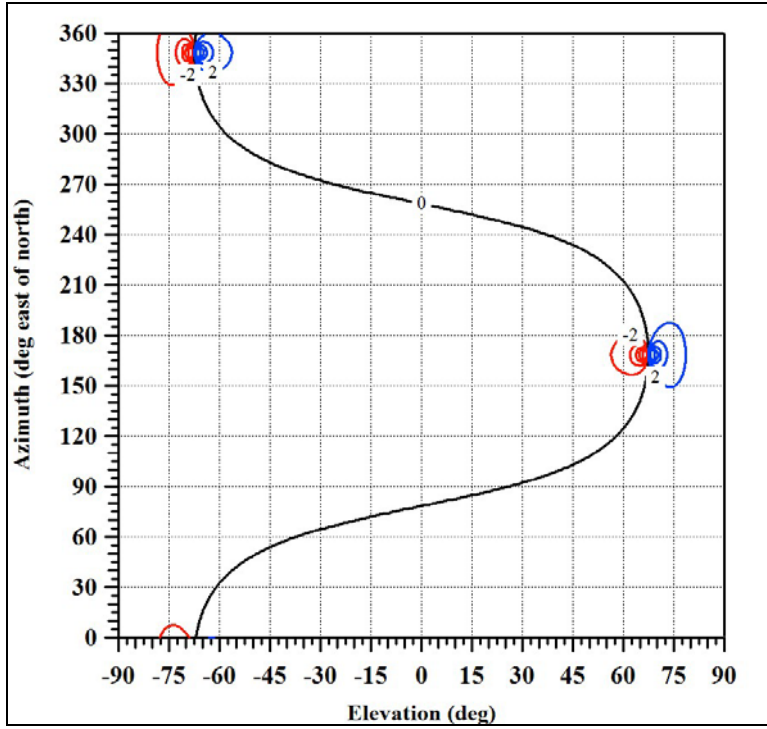


Figure 6. $\partial\phi_M/\partial\psi_N$ at APG.

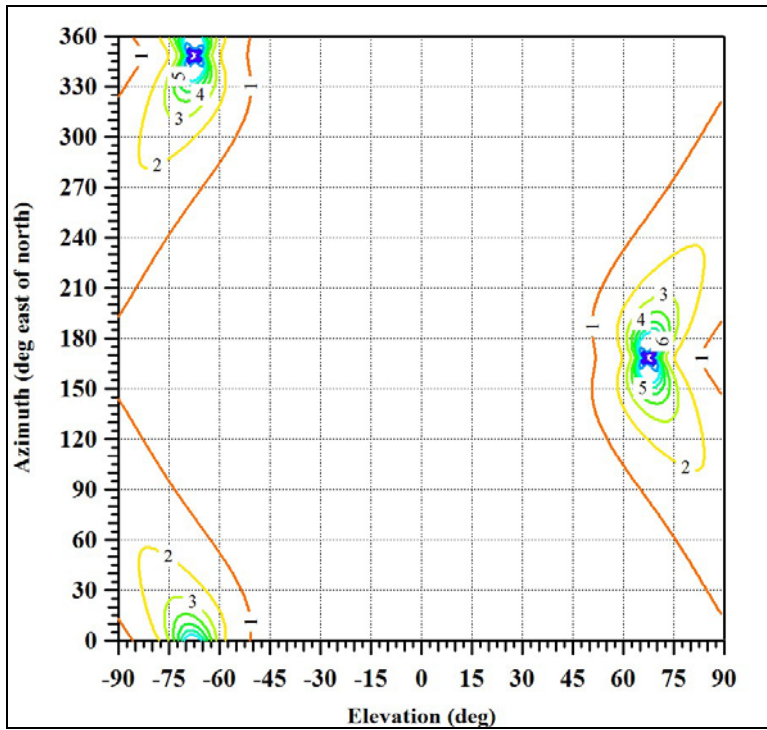


Figure 7. RSS of $\partial\phi_M/\partial\theta$ and $\partial\phi_M/\partial\psi_N$.

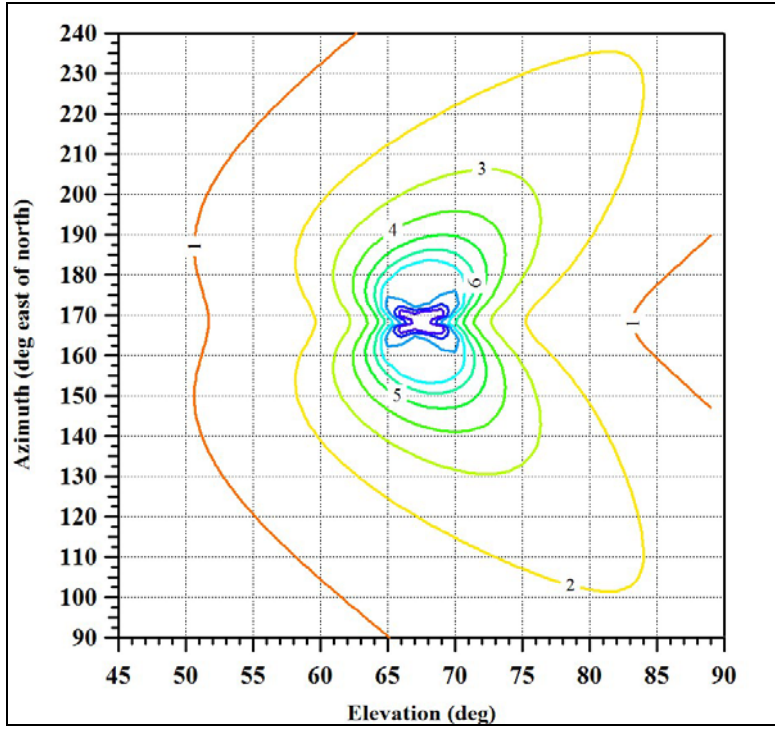


Figure 8. RSS in region of sensitivity.

The implications of these results perhaps can be better appreciated if we consider the statistics in table 1. The cumulative RSS values show that a 1-degree error in the estimates of the independent angular variables, i.e., projectile elevation, projectile azimuth, and/or magnetic field orientation, results in less than a 1-degree error in the roll angle computation in 78% of the possible projectile headings and results in less than a 2-degree error in the roll angle computation in 93% of the possible projectile headings. The statistics in table 1 give the probabilities at the various sensitivity levels when all possible combinations of azimuth and elevation angle are considered. Not all elevation angles are possible for most projectiles of interest to the Army, however.

Table 1. Error sensitivity of roll angle computations.

Error Magnitude	$\partial\phi_M/\partial\theta$	$\partial\phi_M/\partial\psi_N$	RSS	Cumulative RSS
0→1	0.897469	0.752500	0.778673	0.778673
1→2	0.085864	0.117191	0.150463	0.929136
2→3	0.009753	0.080185	0.042685	0.971821
3→4	0.003056	0.023272	0.012901	0.984722
4→5	0.001512	0.009815	0.005463	0.990185
5→6	0.000556	0.005617	0.003148	0.993333
6→7	0.000525	0.002963	0.001852	0.995185
7→8	0.000247	0.001944	0.003056	0.998241
8→9	0.000340	0.001358	0.001019	0.999259
9→10	0.000062	0.000802	0.000185	0.999444
>10	0.000617	0.004352	0.000556	1.000000

In order to compute the sensitivities for a particular application, the range of elevation angles needs to be restricted to those appropriate to that application. For example, artillery projectiles are most often launched at elevation angles less than 60 degrees and tank main guns can only be elevated to approximately 20 degrees. When the range of elevation angles is restricted to $-75 \text{ degrees} \leq \theta \leq 60 \text{ degrees}$ for artillery and restricted to $-30 \text{ degrees} \leq \theta \leq 20 \text{ degrees}$ for tank main guns, the probabilities given in table 2 resulted for potential artillery and tank projectile headings and the geo-magnetic field at APG. The decrease in error sensitivity for the artillery rounds is because some portion of the region of greater sensitivity at APG is outside the elevation angle boundaries of these projectiles. The potential range of tank-gun-launched projectiles' elevation angles is far removed from the regions of high error sensitivity at APG, as can be seen from the computed probabilities. These results demonstrate that the expected reliability of magnetic roll orientation determination depends to some degree on the envisioned application.

Table 2. Error sensitivity of roll angle computations for artillery and tanks at APG.

Error Magnitude	Artillery RSS	Artillery Cumulative RSS	Tank RSS	Tank Cumulative RSS
0→1	0.910412	0.910412	1.00	1.00
1→2	0.056543	0.966955	0	1.00
2→3	0.014794	0.981749	0	1.00
3→4	0.008066	0.989815	0	1.00
4→5	0.003642	0.993457	0	1.00
>5	0.002099	1.000000	0	1.00

4. Sensor Survivability

The Honeywell solid state vector magnetometers used at ARL and their supporting electronics were subjected to a range of shock and environmental testing before being included in flight instrumentation packages. These devices have survived and functioned after air gun tests at acceleration levels as great as 100 kg when unpowered. They also have been included on hundreds of flight experiments where the sensors have been powered during launch set-back accelerations as great as 49 kg (figure 9). The 49-kg launch flight test was specifically conducted to evaluate the magnetometer's survivability and functionality in the tank gun environment. Such devices are planned to be used in tank gun ammunition with greater than 75-kg launch accelerations in the near future.

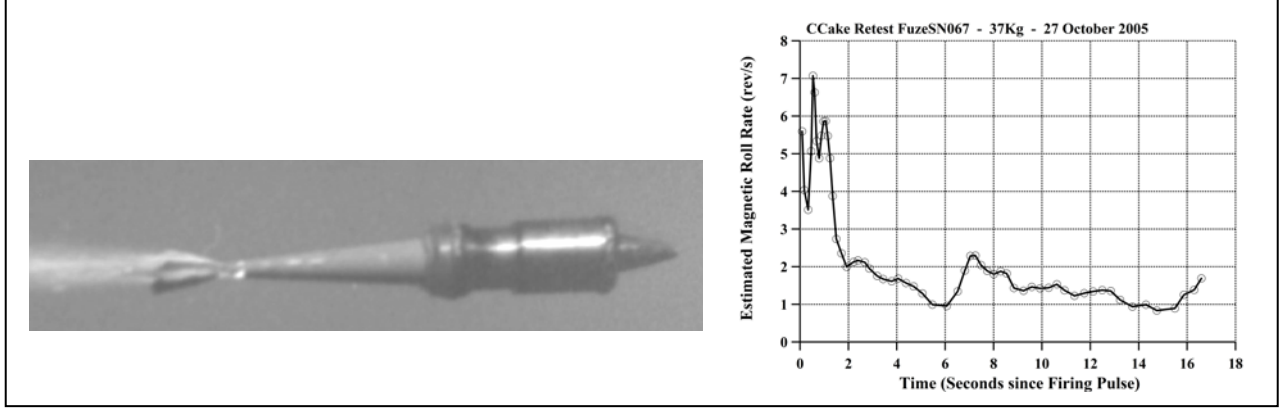


Figure 9. M831 with diagnostic fuze after 49-kg launch and magnetometer-derived roll rate.

5. Real-Time, On-Board Solution of the Roll Equations

Obtaining roll orientation from radial magnetometer data ultimately depends on solving equations 4 and 5 for the angle ϕ . We begin by deriving the explicit, point-wise solution of equation 4 and then discussing alternate solution methods appropriate to particular types of projectile flight characteristics. This discussion is meant to demonstrate that a variety of methods is available for roll orientation estimation with the most appropriate method being application specific.

5.1 Explicit Solution

Solutions of equations 4 and 5 are analogous with appropriate changes of variables. Therefore, we consider only equation 4.

$$m_j = [\sin(\theta) \sin(\phi) \cos(\psi_N) - \cos(\phi) \sin(\psi_N)] m_n + [\sin(\theta) \sin(\phi) \sin(\psi_N) + \cos(\phi) \cos(\psi_N)] m_e + \cos(\theta) \sin(\phi) m_d \quad (4)$$

Rearranging terms gives

$$m_j = \sin \phi (\sin \theta \cos \psi_N m_n + \sin \theta \sin \psi_N m_e + \cos \theta m_d) + \cos \phi (-\sin \psi_N m_n + \cos \psi_N m_e) \quad (7)$$

After making the substitution $Q = \tan \frac{\phi}{2}$, we obtain ϕ thus

$$m_j = \frac{2Q}{1+Q^2} (\sin \theta \cos \psi_N m_n + \sin \theta \sin \psi_N m_e + \cos \theta m_d) + \frac{1-Q^2}{1+Q^2} (-\sin \psi_N m_n + \cos \psi_N m_e) \quad (8)$$

$$\begin{aligned}
0 = & Q^2(m_e - \sin \psi_N m_n + \cos \psi_N m_e) \\
& - 2Q(\sin \theta \cos \psi_N m_n + \sin \theta \sin \psi_N m_e + \cos \theta m_d) \\
& + (m_e + \sin \psi_N m_n - \cos \psi_N m_e)
\end{aligned} \tag{9}$$

Letting

$$\begin{aligned}
A &= (m_e - \sin \psi_N m_n + \cos \psi_N m_e) \\
B &= -2(\sin \theta \cos \psi_N m_n + \sin \theta \sin \psi_N m_e + \cos \theta m_d), \\
C &= (m_e + \sin \psi_N m_n - \cos \psi_N m_e)
\end{aligned} \tag{10}$$

yields

$$Q = \frac{-B \pm \sqrt{B^2 - 4AC}}{2A} \quad \text{and finally, } \phi = 2 \tan^{-1}(Q) \tag{11}$$

where the correct root is determined by the polarity of $\frac{\partial m_j}{\partial t}$. If $\frac{\partial m_j}{\partial t} \leq 0$, the correct root is $\frac{-B + \sqrt{B^2 - 4AC}}{2A}$. If $\frac{\partial m_j}{\partial t} > 0$, the correct root is $\frac{-B - \sqrt{B^2 - 4AC}}{2A}$.

The requirements for obtaining this explicit instantaneous solution for ϕ are a calibrated radial magnetometer, knowledge of the local geomagnetic field vector, $\vec{M}_N = (m_n, m_e, m_d)$, and knowledge of the instantaneous projectile elevation (θ) and azimuth (ψ_N) angles. Depending on the weapon system, the projectile's instrumentation, and the projectile's expected dynamics, these requirements can be met in a variety of ways.

In a command-guided system where a projectile and target are being tracked, the heading and magnetic field parameters could be measured and the required intercept maneuver(s) calculated on the ground with a system asset. The timing and radial magnetometer values could then be transmitted to the projectile for use in an on-board guidance, navigation, and control (GNC) processor.

Regarding projectiles where the navigation solution would be computed with an on-board processor, a global positioning system (GPS)-equipped projectile could estimate its own elevation and azimuth angles. The geomagnetic field vector could be downloaded to the projectile before, during, or after projectile launch, depending on launcher and projectile equipment. With knowledge of a projectile's heading and the field vector and sufficient time before roll orientation needs to be known, a radial magnetometer easily could be calibrated in flight on board any projectile whose spin rate is high with respect to its pitching and yawing rates. Alternatively, a processor on a GPS-equipped projectile with a three-axis, calibrated magnetometer and sufficient time could solve for the local field vector before proceeding to the roll angle computations.

Another possibility is for a projectile whose anticipated heading history is well known *a priori*; estimated values of elevation and azimuth as functions of time could be used in lieu of GPS-derived

values. These by no means exhaust the possibilities for an explicit solution of the roll equations but illustrate that many methods are possible and the preferred method should be determined for an individual application.

5.2 Projectile-Dynamics-Dependent Methods

Many inventory and developmental ordnance projectiles have an approximately steady state spin rate or a slowly changing spin rate that is high with respect to the pitching and yawing rates. For such projectiles, it is often unnecessary to explicitly solve for ϕ via the roll equations. If the local field is known and the projectile heading is known or estimable as discussed previously, the projectile roll orientations at the times of Mag_K field crossings can be computed for the current projectile heading with equation 6. Mag_J roll orientations at field crossings can be computed analogously. These solutions provide four roll indices per revolution, which can be identified from the extrema of the m_j and m_k signals. Current spin rate is obtained from period measurements, based on the times of occurrence of these same extrema. Roll orientations at other desired times are obtained by extrapolation from the last index, based on the spin rate. This implementation does not require that the radial magnetometers be calibrated and has been successfully employed in the GNC algorithms in several developmental guided projectiles.

For any spinning projectile with a calibrated three-axis magnetometer whose ballistic trajectory is primarily confined to a vertical plane, both the geomagnetic field vector and the projectile roll orientation can be estimated from magnetometer data alone (Wilson, 2006). In this case, sufficient time is required for a recursive linear least squares solution to converge.

For a projectile whose dynamics combine both these features, i.e., an approximately steady state spin rate or a slowly changing spin rate and a ballistic trajectory that is confined to a vertical plane, the horizontal component of the local field in the earth-fixed coordinate system provides a roll index twice per revolution. This can be seen if we evaluate equation 4 for $\phi = 0$ and $\phi = 180$. When $\phi = 0$, Mag_J is horizontal and oriented to the right when one is looking down range and equation 4 yields

$$\begin{aligned} m_j &= [\sin(\theta)\sin(0)\cos(\psi_N) - \cos(0)\sin(\psi_N)]m_n \\ &\quad + [\sin(\theta)\sin(0)\sin(\psi_N) + \cos(0)\cos(\psi_N)]m_e + \cos(\theta)\sin(0)m_d . \\ &= -\sin(\psi_N)m_n + \cos(\psi_N)m_e \end{aligned} \quad (12)$$

When $\phi = 180$, Mag_J is horizontal and oriented to the left when one is looking down range and equation 4 yields

$$\begin{aligned} m_j &= [\sin(\theta)\sin(180)\cos(\psi_N) - \cos(180)\sin(\psi_N)]m_n \\ &\quad + [\sin(\theta)\sin(180)\sin(\psi_N) + \cos(180)\cos(\psi_N)]m_e + \cos(\theta)\sin(180)m_d . \\ &= \sin(\psi_N)m_n - \cos(\psi_N)m_e \end{aligned} \quad (13)$$

At both orientations, the values for m_j are constant throughout the trajectory and provide roll indices. These same two values will also occur for m_k when that axis is horizontal, thereby providing two additional indices. As before, roll orientations at other desired times are obtained by extrapolation from the last index, based on the spin rate. In this case, calibrated sensors, the horizontal components of the earth's field, and the projectile line of fire are required. Similarly to the explicit solutions, these examples by no means exhaust the possibilities for dynamics-dependent solutions, and the preferred method should be determined for an individual application.

6. Non-Geomagnetic Field Sensor Stimuli

Until now, all the discussion has assumed ideal vector magnetometers whose output is directly related to the projection of the geomagnetic field onto the sensor axes as described by equations 3, 4, and 5. The final question regarding the viability of roll orientation derivation from magnetic sensor data to be addressed in this report is “Do these equations completely describe projectile-borne vector magnetometers’ output?” If not and the sensors are reacting to additional stimuli other than the earth's magnetic field, can the additional contributions be detected and isolated from the contribution attributable to the earth's field?

Throughout a variety of laboratory tests and post-flight analyses of the Honeywell vector magnetometers, we have never observed any measurable effect on these devices’ output because of temperature, shocks, or dynamic g-loads. In short, the output of these devices has only and always been proportional to the magnetic field strength along the sensors’ axes. Unfortunately, in projectile-borne sensors, there are a number of additional potential contributors to the magnetic field strength along the sensor axes besides the local geomagnetic field. These contributors can broadly be described as magnetic fields independent of the projectile and magnetic fields related to the projectile.

6.1 Projectile-Independent Magnetic Fields

Naturally occurring magnetic fields associated with iron magnets and lodestones have been known since ancient times². Evidence of an electromagnetic field was first observed in 1820 by Hans Christian Oersted. If any of these sources were to be close enough to a projectile-borne magnetometer, the local magnetic field would be the vector sum of the geomagnetic field and those associated with all the other sources. In such cases, the geometric relationship between sensor output and the navigation coordinate system would be corrupted.

In October 2006, flight experiments were conducted in ARL's transonic experimental facility at APG to characterize the flight dynamics of a medium caliber projectile as part of a research project

²For example, the magnetic hill at Moncton, New Brunswick.

at ARL. These experiments were conducted within an enclosed range building to eliminate the effects of any winds and to take advantage of the range instrumentation. The projectiles were instrumented with a number of sensors, including a radially oriented magnetometer. Figure 10 shows the magnetometer output from one such flight experiment and figure 11 shows what the output would have been if the same trajectory had been flown outdoors. The sensor output in figure 10 evidences not only the presence of additional magnetic fields besides the geomagnetic field but attenuation of the geomagnetic field within the building. Projectile roll rates were successfully derived from the radial magnetometer data in these indoor flights, but projectile orientation could not be accurately estimated from the magnetometer data. Clearly, magnetometers are not good roll orientation sensors indoors. Without having made any quantitative measurements, I nonetheless expect that magnetometer-based orientation estimation would not be successful within any intensely developed urban environment. This limitation would not necessarily exclude the use of magnetometers because some ordnance projectile trajectories (e.g., mortar and artillery) would likely include portions at sufficient stand-off distances from these magnetic fields. Orientation information derived during these times could be used to maintain roll estimates during periods of magnetometer corruption. This technique has been successfully demonstrated with flight data at ARL.

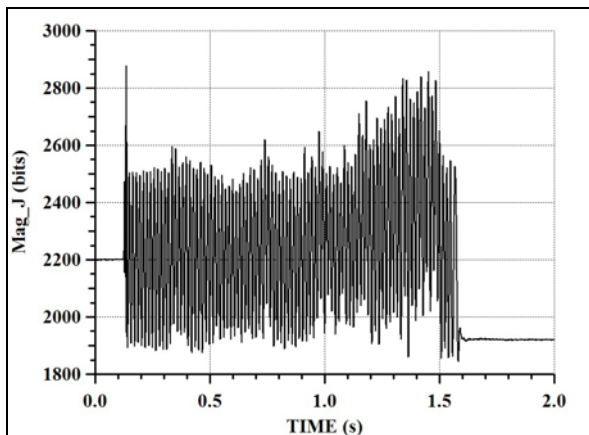


Figure 10. Mag_J output inside range.

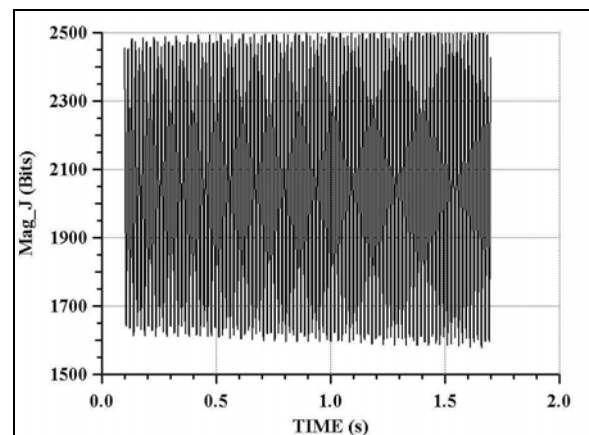


Figure 11. Mag_J output outdoors.

In a laboratory measurement taken during calibration procedures for a fuze-configured instrumentation package (see figure 12), effects of an external electromagnetic field were observed in recorded sensor data (figure 13). This and other similar instrumentation packages are generically referred to as diagnostic fuzes or DFuzes (Davis et al., 2004) and are often used in flight experiments to characterize air frame and GNC system performance. In this particular procedure, a DFuze was attached to a large direct current spin motor to calibrate some spin rate sensors. After data recording began, the motor was powered and the fuze began to spin at an ever-increasing rate until the power was turned off. The motor was then allowed to de-spin until it stopped, whereupon recording was terminated. Magnetometer data evidenced both a growth in amplitude with

spin rate and a bias shift at the instant the power was turned off. Since these effects were observed, ARL has performed subsequent spin calibration measurements using a pneumatic motor.



Figure 12. Diagnostic fuze.

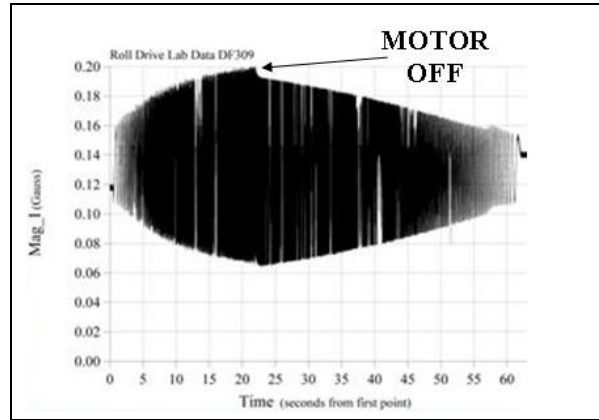


Figure 13. Magnetometer data taken with spin motor.

6.2 Projectile-Related Magnetic Fields

Electromagnetic and naturally occurring fields are of concern for magnetometers embedded within projectiles. Additionally, other magnetically related properties of the materials from which any given projectile is manufactured can and will affect sensor output. Most military ordnance projectiles are made (at least in part) of metal of some kind. Many of these metals have static and dynamic magnetic properties that are of concern for embedded magnetometer performance. Among the static properties, some metals (e.g., ferrous irons) are capable of being magnetized. Figure 14 shows radial magnetometer data from a flight experiment where the sensor was installed within a cylindrical section made of ferrous steel. The sensor offset and gain were intended to center the sensor output signal in the 0- to 6.5-volt range, but the unanticipated permanent magnetism of the ferrous body created a signal bias that resulted in the roll-modulated signal from the geomagnetic field being saturated at the upper end.

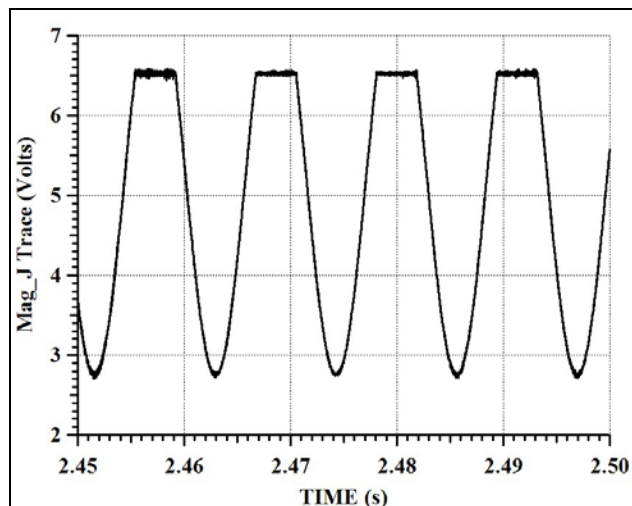


Figure 14. Magnetometer saturation attributable to projectile permanent magnetism.

Permeability is another static material property to be considered. In a laboratory experiment where two magnetometers were placed in a rotating magnetic field with one sensor in the open and the second within a ferrous cylinder, the data shown in figure 15 were recorded. Both sensors had similar gains. The black curve is the output from the sensor in the open and the red curve is the output from the embedded sensor. The field strength along the axis of the embedded sensor is attenuated by almost an order of magnitude. Besides the obvious prohibition of embedding magnetic sensors within impermeable materials (e.g., μ metals), material permeability clearly needs to be considered for any application where magnetic field strength is going to be measured with embedded sensors.

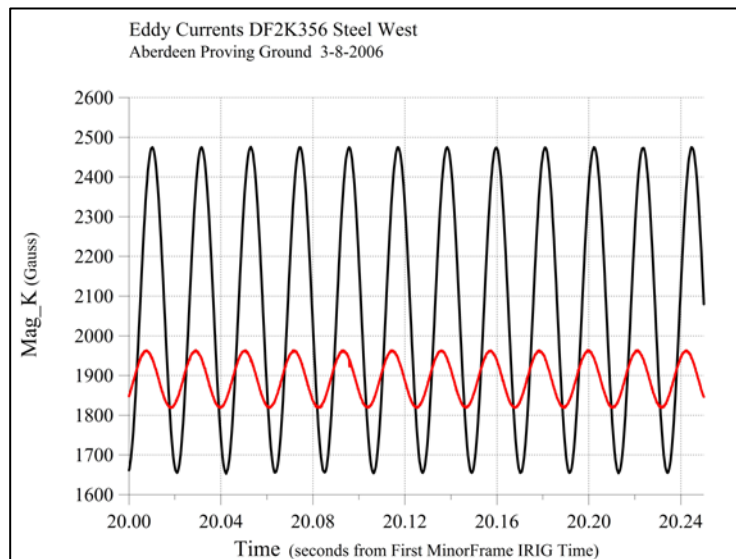


Figure 15. Two magnetometers in a rotating field.

Electromagnetic fields generated by on-board power sources and electrical components can be sources of magnetic sensor corruption. Small electric motors such as that seen in figure 16 are used for canard control in a number of guided projectiles and can create significant magnetic fields. When possible, magnetic sensors should be isolated from these electromagnetic fields by distance or by shielding. When this kind of packaging solution is not achievable, it may still be possible to compensate for the electrically generated fields because they would presumably be predictable and knowable. To date, corruption of this type has never been observed in any flight experiments at ARL.

The depth to which a magnetic field penetrates materials also has a frequency dependency, as can be seen in figure 17. The propagation rate of the external field through these materials also varies directly with frequency. Thus, the output signal of a magnetometer enclosed within a body made from any of these materials would attenuate and lag with spin rate.

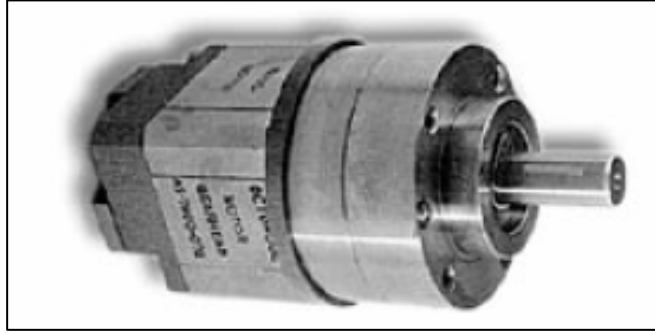


Figure 16. Canard control motor.

When electrical conductors are moved within a magnetic field, electric current is generated within these conductors and additional magnetic fields result. The potential effects of induced current on magnetometer output can be seen in figure 18 (Perry & Jones, 1978). This figure shows the effects of induced eddy currents on the external and internal flux distribution when a permeable solid cylindrical shaft is rotated in a stationary magnetic field. This chart illustrates the effect of projectile rotation on the internal field that an embedded sensor might “see”. The parameter R_m is called the magnetic Reynolds number and is a standard measure of a material’s susceptibility to these eddy current effects. Figure 18 shows the flux distribution for increasing magnetic Reynolds numbers at a constant frequency, but a similar progression of field deformations would apply to a constant material at increasing spin frequencies. Thus, the output signal of a magnetometer exposed to these effects would attenuate and lag in roll angle orientation with respect to the external field.

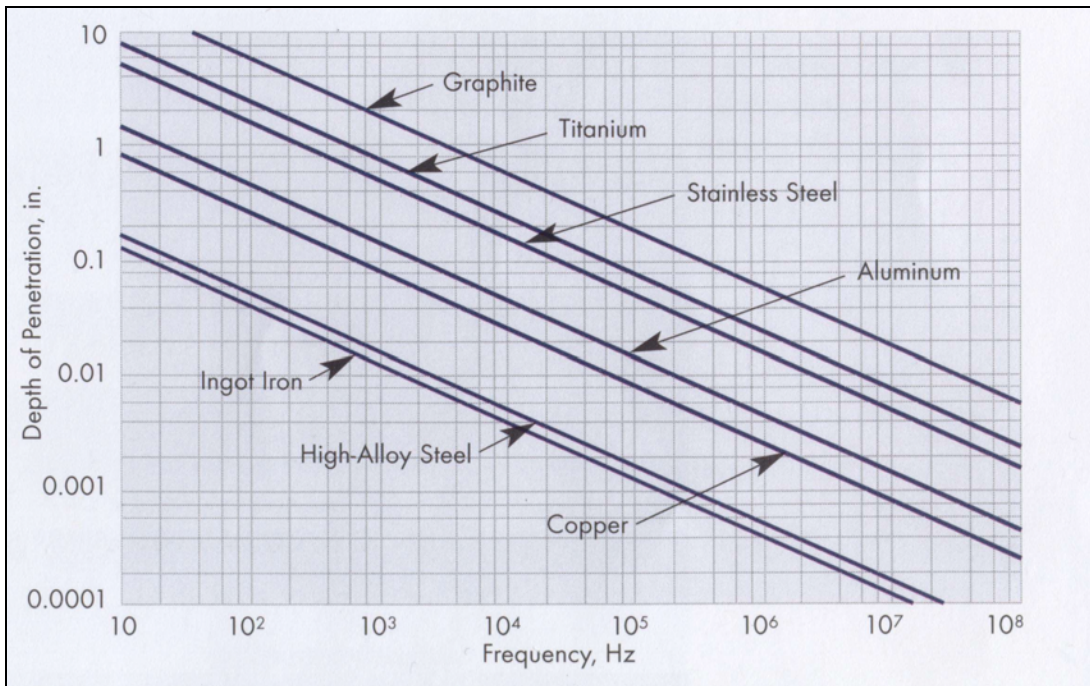


Figure 17. Depth of penetration as a function of frequency.

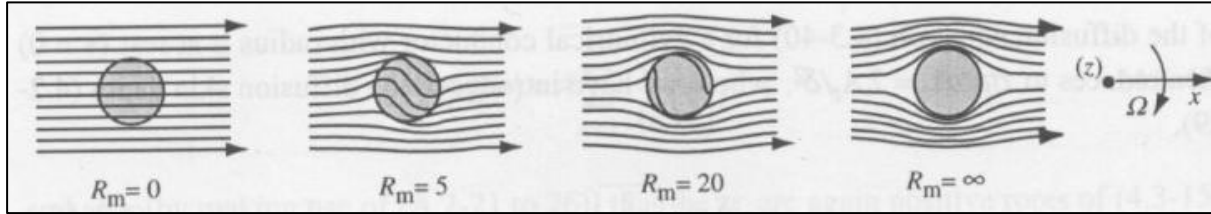


Figure 18. Flux in and around a solid cylinder rotating in a stationary magnetic field.

Although the degrading effects on magnetometer performance of external fields, static magnetic properties, and on-board electronics seem to be reasonably avoidable or capable of correction, dynamic effects such as eddy currents are certainly not avoidable because they are inherent in many of the materials from which ordnance projectiles are necessarily made. In order to experimentally evaluate the feasibility of correcting for these types of effects, a specially configured DFuze with two three-axis magnetometers and a number of test fixtures were designed and manufactured at ARL. The two magnetometers were placed near the fuze centerline at the longitudinal locations indicated by the dots on figure 19. A right cylindrical test fixture into which the DFuze would be threaded and which would itself thread into a pneumatic spin motor was designed. This design is shown in figure 20. When the DFuze is fully screwed into the cylinder, the magnetometer at the aft end of the DFuze is embedded approximately 2 inches within the cylinder and the forward magnetometer is approximately 1 inch forward of the cylinder. Cylinders of this geometry were machined from plastic, aluminum, hardened steel, and stainless steel with at least two copies made for each of the metal cylinders. The tests were conducted outside, far removed from potential corruptors of the geomagnetic field with the DFuze installed on each of the cylinders in turn. Typically, data recording began, air was supplied to the motor to begin spin-up, the air was shut off at some point, the apparatus was allowed to de-spin, and data recording was then stopped. Data were taken on multiple occasions and at different orientations of the air motor with respect to the geomagnetic field.

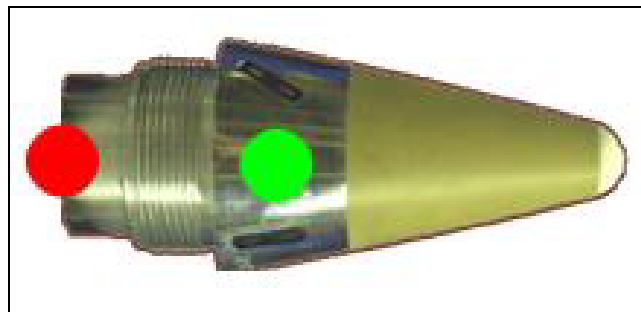


Figure 19. DFuze with two magnetometers.

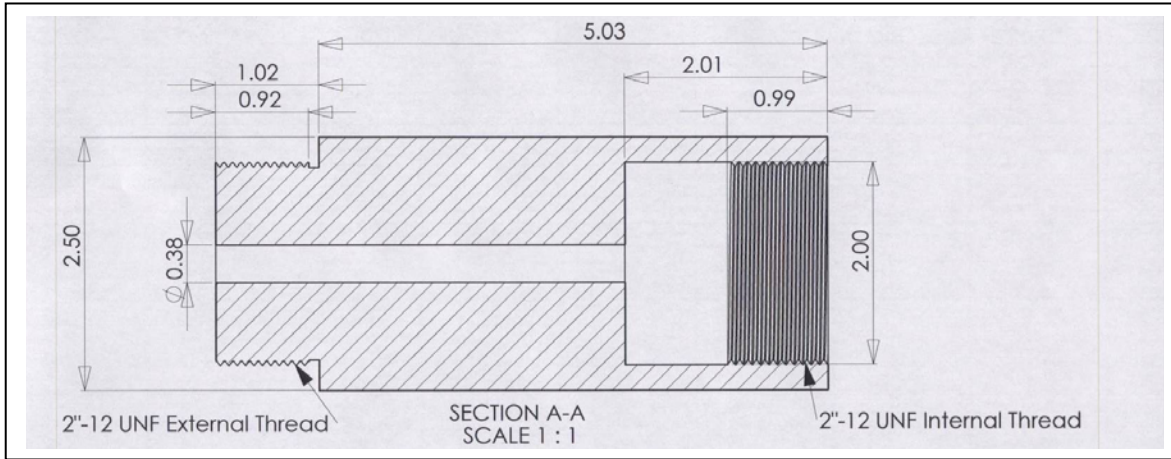


Figure 20. Cylindrical test fixture specifications.

Representative data showing the amplitude effect of spin rate on magnetometer output are shown in figure 21. These data are for one of the aluminum cylinders. The left-most plot gives the spin rate as a function of time for a 65-second interval. The spin is seen to apparently linearly accelerate to a peak rate of nearly 60 revolutions per second at about 19 seconds and then to more slowly decay after the air is turned off. Although they may look like Rohrshach test cards, the radial magnetometer output graphed in the center and right-most plots are actually sinusoids whose frequency is so high that the individual roll periods are indistinguishable on this scale. The important observation to make is that the envelope of the data for the external magnetometer is constant and the envelope of the data for the embedded magnetometer decreases with spin rate. The magnitude of this rate dependency was the same for both aluminum cylinders. Analogous results were obtained for the other metal cylinders, and no effect on amplitude was observed for the plastic cylinder.

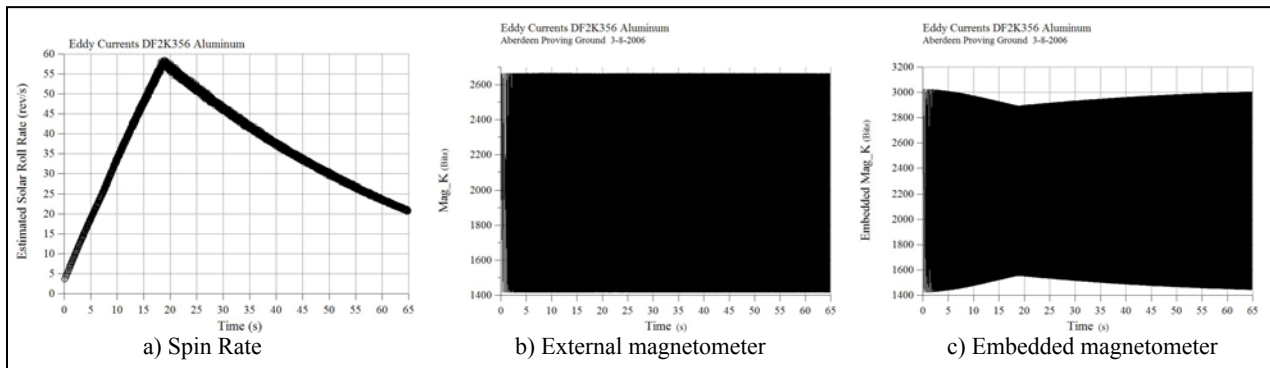


Figure 21. Effect of spin rate on magnetometer output amplitude.

In order to evaluate the effect of spin rate on magnetometer output lag, an inertially stable roll index was required for comparison with magnetometer-derived roll information. This was provided by output from the four optical sensors placed around the DFuze circumference at the same longitudinal location as the external magnetometer. Two of these sensors can be seen in figure 19, one

on either side of the green dot. These sensors are designed to have essentially no output unless aligned with a bright light (in our case, the sun). The polarity and gain of each of the four sensors are varied so the sun crossings for each individual sensor can be identified. Although the sun is constantly moving relative to the earth, for a spin test of approximately 1 minute duration, the sun position is essentially fixed. Because orientation of the spin axis was fixed throughout each test and the solar sensor system has no appreciable latencies, the solar crossings provided reliable roll indices. We eliminated differences in sun position among the individual tests by normalizing all the data through bias shifting of the roll angle at the solar crossing to the geometric roll angle of the geomagnetic field crossing.

Figure 22 shows a representative sample of data from the embedded magnetometer (black curve) and the solar sensors (red curve) for an experiment with the DFuze installed on an aluminum cylinder. In each projectile roll period, there are four spikes on the solar sensor curve. The larger amplitude, positive spike (solar sensor 1) was used as the roll index; each roll period began at the crossing time of solar sensor 1; the roll rate was estimated by the reciprocal of the times between successive crossings of solar sensor 1. Within each roll period, the roll orientation was estimated from the time at which the magnetometer maximum occurred between the times of the neighboring solar sensor crossings. After the data from several tests with different cylinders at different times were normalized, these relative roll orientation measurements were plotted versus spin rate (figure 23). This plot provides a direct comparison of the spin rate-related lags for the four materials from which cylinders were made.

The output from the external magnetometer, labeled “Mag in Fuze Body” on figure 23, has some lag because the DFuze body used in these experiments is made from aluminum. In the near future, ARL hopes to design and build a sensor housing made with plastic or some other suitable material with no static or dynamic magnetic properties that affect embedded sensor output. In figure 23, the plastic-embedded sensor output is the same as that from the external sensor. The aluminum, hardened steel, and stainless steel embedded sensors each have lag to different degrees. Figure 24 shows the analogous results from data taken for two of the three stainless steel cylinders. This plot demonstrates the crucial result supported by all the experiments conducted to date that the dynamic magnetometer-output-affecting phenomenologies are repeatable for the same materials within the manufacturing tolerances of the test cylinders.

In the tests conducted thus far, there has been no evidence of any other independent variable contributing to dynamic magnetometer output effects besides spin rate and cylinder/projectile materials. When the new sensor housing is made, ARL plans to undertake a test matrix of materials, field strengths, and spin rates that will hopefully support this conclusion. If this proves to be true, we can easily compensate for these effects by measuring spin rate and applying appropriate corrections to magnetometer output in both amplitude and lag. With these corrections, the orientation measurements described in section 5 can be realized.

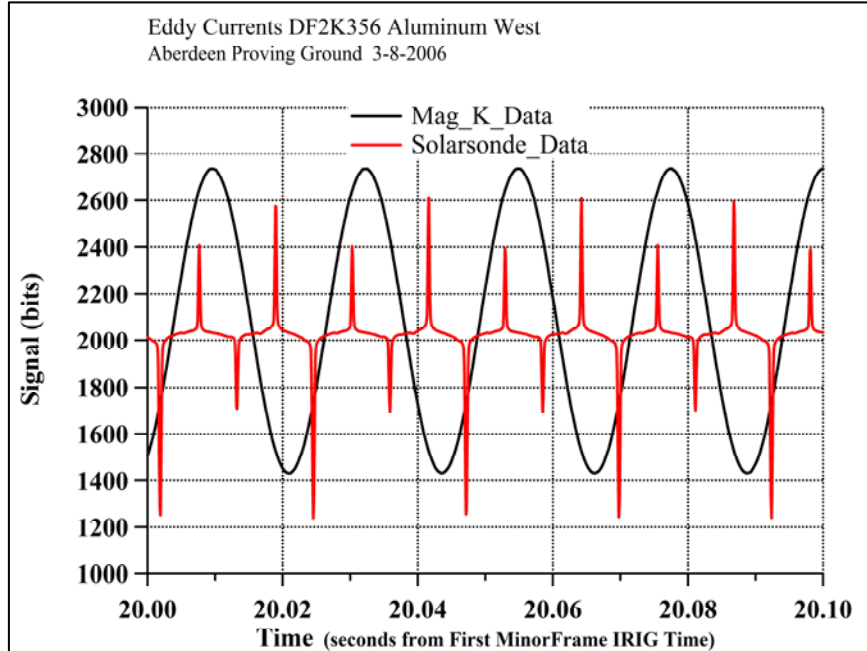


Figure 22. Representative magnetic and solar sensor data from spin effects tests.

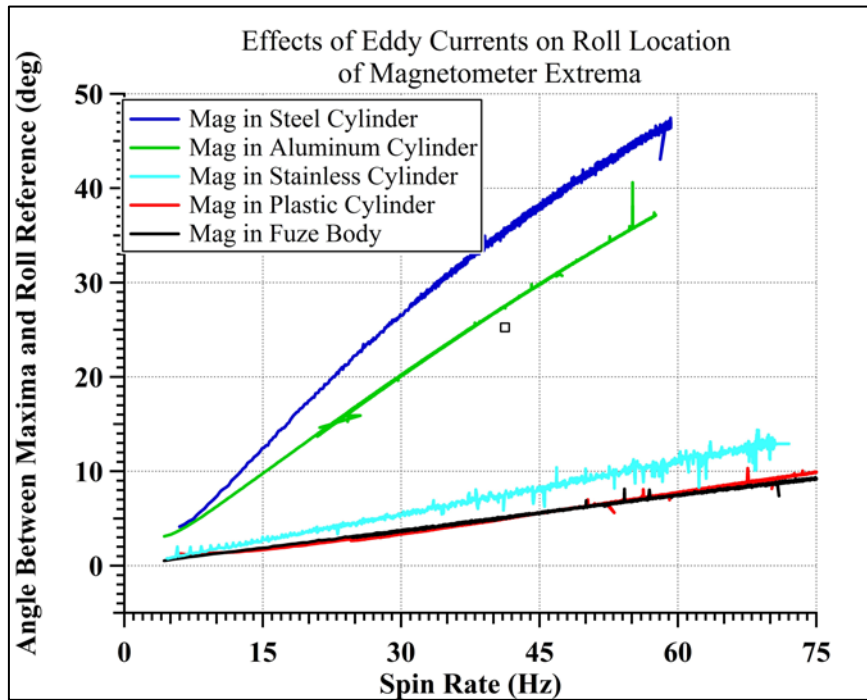


Figure 23. Magnetometer output lag versus spin rate for various materials.

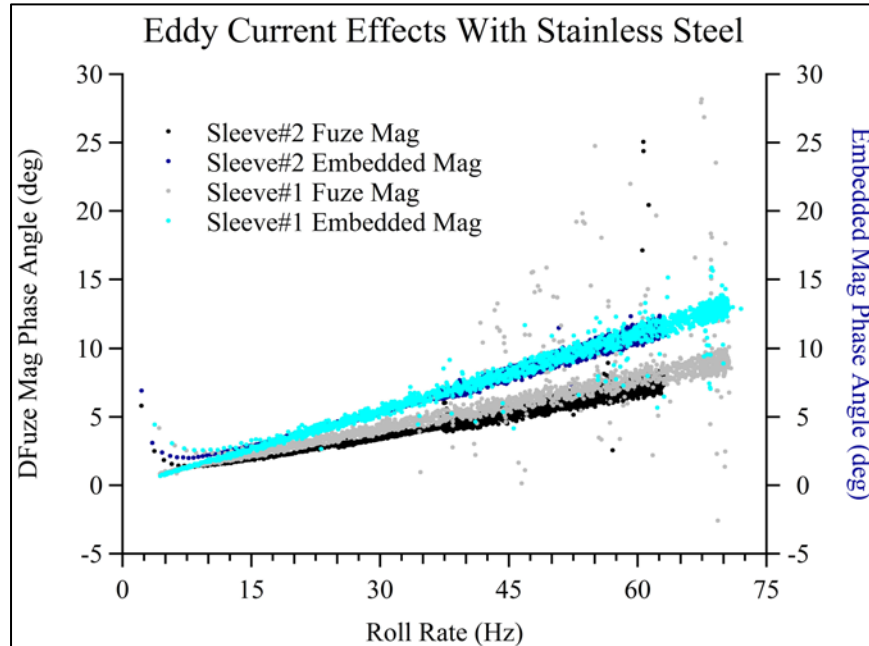


Figure 24. Embedded magnetometer lags for two stainless steel cylinders.

In a projectile development program conducted during 2006 (Struck, 2007), ground measurements of magnetometer output lag were made with an apparatus capable of spinning the entire free-flight projectiles. Sensor data such as those seen in figures 23 and 24 were collected, and lag corrections based on these measurements were implemented in the on-board maneuver mechanism control algorithm. Each of the five test projectiles maneuvered in the desired directions. This result, combined with the repeatability demonstrated in figure 24, provides evidence that supports the possibility of making a representative ground measurement to characterize and effectively compensate for dynamic magnetic effects for all similar projectiles.

7. Summary

The mathematics of achieving usable orientation estimates from embedded vector magnetometer output depend on accurate determinations of the projections of the geomagnetic field onto the magnetic sensors' axes. These sensors' output are potentially affected by stimuli other than the geomagnetic field. In every ground and flight experiment conducted to date, the projections of the geomagnetic field onto the magnetic sensors' axes could be determined if the other stimuli were eliminated or if the other stimuli were compensated. Further testing and analyses are necessary before these results can be termed definitive, but I am at this time optimistic that magnetometric orientation estimation can be a viable component of a low-cost projectile GNC system.

8. References

- Davis, B.; Harkins, T.; Hepner, D.; Patton, B.; Hall, R. *Aeroballistic Diagnostic Fuze (DFuze) Measurements for Projectile Development, Test, and Evaluation*; ARL-TR-3204; U.S. Army Research Laboratory: Aberdeen Proving Ground, MD, July 2004.
- Harkins, T. *Understanding Body-Fixed Sensor Output From Projectile Flight Experiments*; ARL-TR-3029; U.S. Army Research Laboratory: Aberdeen Proving Ground, MD, August 2003.
- Harkins, T. *Using Magnetometers for Roll Position Determination in a Spinning Projectile Control System: Theory and Flight Test Results*; ARL-TR-3142; U.S. Army Research Laboratory: Aberdeen Proving Ground, MD, March 2004.
- Harkins, T. *Solving for Flight Body Angular Histories With the Use of Solar and Magnetic Sensor Data*; ARL-TR-4072; U.S. Army Research Laboratory: Aberdeen Proving Ground, MD, April 2007.
- Hepner, D.; Harkins, T. *Determining Inertial Orientation of a Spinning Body With Body-Fixed Sensors*; ARL-TR-2313; U.S. Army Research Laboratory: Aberdeen Proving Ground, MD, January 2001.
- Perry, M.; Jones, T.; *Eddy Current Induction in a Solid Conducting Cylinder with a Transverse Magnetic Field*; IEEE Transactions on Magnetics, Vol. MAG-14, No. 4, July 1978.
- Struck, J. Private communication of data from U.S. Army Armaments Research, Development, and Engineering Center: Picatinny Arsenal, NJ; February 2007.
- Wilson, M. *Attitude Determination With Magnetometers for Gun-Launched Munitions*; ARL-TR-3209; U.S. Army Research Laboratory: Aberdeen Proving Ground, MD, August 2004.
- Wilson, M. *Flight Parameter Estimation With Magnetometers for Precision Guided Mortar Munitions*; ARL-TR-3574; U.S. Army Research Laboratory: Aberdeen Proving Ground, MD, August 2005.
- Wilson, M. *Precision Guided Mortar Munition (PGMM) Roll Angle Determination With the Use of On-line Magnetic Field Estimation*; ARL-TR-3732; U.S. Army Research Laboratory: Aberdeen Proving Ground, MD, March 2006.

NO. OF
COPIES ORGANIZATION

1 DEFENSE TECHNICAL
(PDF INFORMATION CTR
Only) DTIC OCA
8725 JOHN J KINGMAN RD
STE 0944
FORT BELVOIR VA 22060-6218

1 US ARMY RSRCH DEV & ENGRG CMD
SYSTEMS OF SYSTEMS
INTEGRATION
AMSRD SS T
6000 6TH ST STE 100
FORT BELVOIR VA 22060-5608

1 DIRECTOR
US ARMY RESEARCH LAB
IMNE ALC IMS
2800 POWDER MILL RD
ADELPHI MD 20783-1197

1 DIRECTOR
US ARMY RESEARCH LAB
AMSRD ARL CI OK TL
2800 POWDER MILL RD
ADELPHI MD 20783-1197

2 DIRECTOR
US ARMY RESEARCH LAB
AMSRD ARL CI OK T
2800 POWDER MILL RD
ADELPHI MD 20783-1197

3 DIR US ARMY RSCH LABORATORY
ATTN AMSRD ARL SE RL M DUBEY
B PIEKARSKI
AMSRD ARL SE EE Z SZTANKAY
2800 POWDER MILL RD
ADELPHI MD 20783-1197

2 DIR US ARMY RSCH LABORATORY
ATTN AMSRD ARL SE S J EICKE
AMSRD ARL SE SA J PRICE
2800 POWDER MILL RD
ADELPHI MD 20783-1197

3 DIR US ARMY RSCH LABORATORY
ATTN AMSRD ARL SE SS LADAS
A EDELSTEIN D FLIPPEN
2800 POWDER MILL RD
ADELPHI MD 20783-1197

1 DIR US ARMY RSCH LABORATORY
ATTN AMSRD ARL WM MB A FRYDMAN
2800 POWDER MILL RD
ADELPHI MD 20783-1197

NO. OF
COPIES ORGANIZATION

5 CDR US ARMY TACOM ARDEC
ATTN AMSRD AAR AEP F(A) W KONICK
C ROBINSON M D'ONOFRIO
D WARD B CHRISTOPHERSON
2800 POWDER MILL RD
ADELPHI MD 20783-1197

1 DIR US ARMY CECOM RDEC
ATTN AMSEL RD C2 CS J VIG
FORT MONMOUTH NJ 07703-5601

1 CDR US ARMY TACOM ARDEC
ATTN AMSRD AAR QEM E M BOMUS
BLDG 65S
PICATINNY ARSENAL NJ 07806-5000

4 CDR US ARMY TACOM ARDEC
ATTN AMSRD AAR AEM A S CHUNG
W KOENIG W TOLEDO
T RECCHIA
BLDG 95
PICATINNY ARSENAL NJ 07806-5000

1 CDR US ARMY TACOM ARDEC
ATTN AMSRD AAR AEM A F BROWN
BLDG 151
PICATINNY ARSENAL NJ 07806-5000

1 CDR US ARMY TACOM ARDEC
ATTN AMSRD AAR AEM C A MOCK
BLDG 171A
PICATINNY ARSENAL NJ 07806-5000

1 CDR US ARMY TACOM ARDEC
ATTN AMSRD AAR AEM C J POTUCEK
BLDG 61S
PICATINNY ARSENAL NJ 07806-5000

1 CDR US ARMY TACOM ARDEC
ATTN AMSRD AAR AEP S PEARCY
BLDG 94
PICATINNY ARSENAL NJ 07806-5000

1 CDR US ARMY TACOM ARDEC
ATTN AMSRD AAR AEP M CILLI
BLDG 382
PICATINNY ARSENAL NJ 07806-5000

5 CDR US ARMY TACOM ARDEC
ATTN AMSRD AAR AEP E J VEGA
P GRANGER D CARLUCCI
M HOLLIS J KALINOWSKI
BLDG 94
PICATINNY ARSENAL NJ 07806-5000

NO. OF
COPIES ORGANIZATION

7 CDR US ARMY TACOM ARDEC
ATTN AMSRD AAR AEP E D TROAST
BLDG 171
PICATINNY ARSENAL NJ 07806-5000

2 CDR US ARMY TACOM ARDEC
ATTN AMSRD AAR AEP F H RAND
BLDG 61S
PICATINNY ARSENAL NJ 07806-5000

2 CDR US ARMY TACOM ARDEC
ATTN AMSRD AAR AEP F D PASCUA
BLDG 65S
PICATINNY ARSENAL NJ 07806-5000

2 CDR US ARMY TACOM ARDEC
ATTN AMSRD AAR AEP I
S LONGO C HALKIAS
BLDG 65S
PICATINNY ARSENAL NJ 07806-5000

4 CDR US ARMY TACOM ARDEC
ATTN AMSRD AAR AEP S N GRAY
M MARSH Q HUYNH
T ZAPATA
BLDG 94
PICATINNY ARSENAL NJ 07806-5000

1 CDR US ARMY TACOM ARDEC
ATTN AMSRD AAR AEP S C PEREIRA
BLDG 192
PICATINNY ARSENAL NJ 07806-5000

5 CDR US ARMY TACOM ARDEC
ATTN AMSRD AAR AEM L
M LUCIANO
G KOLASA M PALATHINGAL
D VO A MOLINA
BLDG 65S
PICATINNY ARSENAL NJ 07806-5000

1 CDR US ARMY TACOM ARDEC
ATTN AMSRD AAR AEM L R CARR
BLDG 1
PICATINNY ARSENAL NJ 07806-5000

1 CDR US ARMY TACOM ARDEC
ATTN AMSRD AAR AEM L J STRUCK
BLDG 472
PICATINNY ARSENAL NJ 07806-5000

NO. OF
COPIES ORGANIZATION

1 CDR US ARMY TACOM ARDEC
ATTN SFAE SDR SW IW B D AHMAD
BLDG 151
PICATINNY ARSENAL NJ 07806-5000

1 CDR US ARMY TACOM ARDEC
ATTN SFAE AMO CAS EX C GRASSANO
BLDG 171A
PICATINNY ARSENAL NJ 07806-5000

3 PRODUCT MANAGER FOR MORTARS
ATTN SFAE AMO CAS MS G BISHOP
P BURKE D SUPER
BLDG 162 SOUTH
PICATINNY ARSENAL NJ 07806-5000

1 PRODUCT MANAGER FOR MORTARS
ATTN SFAE AMO CAS MS J TERHUNE
BLDG 354
PICATINNY ARSENAL NJ 07806-5000

3 CDR US ARMY TACOM ARDEC
ATTN SFAE AMO CAS R KIEBLER
M MORATZ A HERRERA
BLDG 171A
PICATINNY ARSENAL NJ 07806-5000

3 CDR NAVAL SURF WARFARE CTR
ATTN G34 M TILL G34 H WENDT
G34 M HAMILTON
G34 S CHAPPELL
17320 DAHLGREN ROAD
DAHLGREN VA 22448-5100

3 CDR NAVAL SURF WARFARE CTR
ATTN G34 J LEONARD
G34 W WORRELL
G34 M ENGEL
17320 DAHLGREN ROAD
DAHLGREN VA 22448-5100

4 CDR NAVAL SURF WARFARE CTR
ATTN G61 E LARACH G61 M KELLY
G61 A EVANS
17320 DAHLGREN ROAD
DAHLGREN VA 22448-5100

1 CDR OFC OF NAVAL RSCH
ATTN CODE 333 P MORRISSON
800 N QUINCY ST RM 507
ARLINGTON VA 22217-5660

NO. OF
COPIES ORGANIZATION

1 DIR NAVAL AIR SYSTEMS CMD
TEST ARTICLE PREP DEP
ATTN CODE 5 4 R FAULSTICH
BLDG 1492 UNIT 1
47758 RANCH RD
PATUXENT RIVER MD 20670-1456

1 CDR NAWC WEAPONS DIV
ATTN CODE 543200E G BORGEN
BLDG 311
POINT MUGU CA 93042-5000

2 PROGRAM MANAGER ITTS
PEO-STRI
ATTN AMSTI EL D SCHNEIDER
C GOODWIN
12350 RESEARCH PKWY
ORLANDO FL 32826-3276

2 CDR US ARMY RDEC
ATTN AMSRD AMR SG SD P JENKINS
AMSRD AMR SG SP P RUFFIN
BLDG 5400
REDSTONE ARSENAL AL 35898-5247

1 DIR US ARMY RTTC
ATTN STERT TE F TD R EPPS
REDSTONE ARSENAL AL 35898-8052

1 ARROW TECH ASSOCIATES
ATTN W HATHAWAY
1233 SHELBURNE RD STE 8
SOUTH BURLINGTON VT 05403

5 ALLIANT TECHSYSTEMS
ATTN A GAUZENS J MILLS
B LINDBLOOM E KOSCO
D JACKSON
PO BOX 4648
CLEARWATER FL 33758-4648

1 ALLIANT TECHSYSTEMS
ATTN R DOHRN
5050 LINCOLN DR
MINNEAPOLIS MN 55436-1097

5 ALLIANT TECHSYSTEMS
ATTN G PICKUS F HARRISON
M WILSON (3 CYS)
4700 NATHAN LANE NORTH
PLYMOUTH MN 55442

NO. OF
COPIES ORGANIZATION

8 ALLIANT TECHSYSTEMS
ALLEGANY BALLISTICS LAB
ATTN S OWENS C FRITZ J CONDON
B NYGA
J PARRILL M WHITE
S MCCLINTOCK K NYGA
MAIL STOP WV01-08 BLDG 300
RM 180
210 STATE ROUTE 956
ROCKET CENTER WV 26726-3548

2 SAIC
ATTN J DISHON
16701 W BERNARDO DR
SAN DIEGO CA 92127

3 SAIC
ATTN J GLISH J NORTHRUP
G WILLENBRING
8500 NORMANDALE LAKE BLVD
SUITE 1610
BLOOMINGTON MN 55437-3828

1 SAIC
ATTN D HALL
1150 FIRST AVE SUITE 400
KING OF PRUSSIA PA 19406

1 AAI CORPORATION
M/S 113/141
ATTN C BEVARD
124 INDUSTRY LANE
HUNT VALLEY MD 21030

2 JOHNS HOPKINS UNIV
APPLIED PHYSICS LABORATORY
ATTN W D'AMICO K FOWLER
1110 JOHNS HOPKINS RD
LAUREL MD 20723-6099

4 CHLS STARK DRAPER LAB
ATTN J CONNELLY J SITOMER
T EASTERLY A KOUREPENIS
555 TECHNOLOGY SQUARE
CAMBRIDGE MA 02139-3563

2 ECIII LLC
ATTN R GIVEN J SWAIN
BLDG 2023E
YPG AZ 85365

NO. OF
COPIES ORGANIZATION

- 1 GD-OTS
ATTN E KASSHEIMER
PO BOX 127
RED LION PA 17356
- 1 ALION SCIENCE
ATTN P KISATSKY
12 PEACE RD
RANDOLPH NJ 07861
- ABERDEEN PROVING GROUND
- 1 DIRECTOR US ARMY RSCH
LABORATORY
ATTN AMSRD ARL CI OK (TECH LIB)
BLDG 4600
- 1 DIRECTOR US ARMY RSCH
LABORATORY
ATTN AMSRD ARL SG
T ROSENBERGER
BLDG 4600
- 17 DIR USARL
ATTN AMSRD ARL WM BA D LYON
T BROWN E BUKOWSKI
J CONDON B DAVIS
R HALL T HARKINS (5 CYS)
D HEPNER G KATULKA
T KOGLER P MULLER
B PATTON P PEREGINO
BLDG 4600
- 3 DIR USARL
ATTN AMSRD ARL WM BC
P PLOSTINS
B GUIDOS P WEINACHT
BLDG 390
- 3 DIR USARL
ATTN AMSRD ARL WM BD M NUSCA
J COLBURN T COFFEE
BLDG 390
- 2 DIR USARL
ATTN AMSRD ARL WM BF
W OBERLE A THOMPSON
BLDG 390
- 2 DIR USARL
ATTN AMSRD ARL WM MB
J BENDER W DRYSDALE
BLDG 390

NO. OF
COPIES ORGANIZATION

- 2 DIR USARL
ATTN AMSRD ARL WM T B BURNS
ATTN AMSRD ARL WM TC R COATES
BLDG 309
- 4 CDR US ARMY TACOM ARDEC
ATTN AMSRD AAR AEF T
R LIESKE J MATTS
F MIRABELLE J WHITESIDE
BLDG 120
- 2 CDR ABERDEEN TEST CENTER
ATTN CSTE DTC AT TD B
K MCMULLEN
CSTE DTC AT SL B D DAWSON
BLDG 359
- 2 CDR ABERDEEN TEST CENTER
ATTN CSTE DTC AT FC L R SCHNELL
J DAMIANO
BLDG 400
- 1 CDR ABERDEEN TEST CENTER
ATTN CSTE DTC AT TD S WALTON
BLDG 359
- 1 CDR USAEC
ATTN CSTE AEC SVE B D SCOTT
BLDG 4120